Volumetric Segmentation Using Weibull E-SD Fields

Jiuxiang Hu, Anshuman Razdan, *Member*, *IEEE*, Gregory M. Nielson, *Senior Member*, *IEEE*, Gerald E. Farin, D. Page Baluch, and David G. Capco

Abstract—This paper presents a coarse-grain approach for segmentation of objects with gray levels appearing in volume data. The input data is on a 3D structured grid of vertices $v(i,j,k)$, each associated with a scalar value. In this paper, we consider a voxel as a $\kappa \times \kappa \times \kappa$ cube and each voxel is assigned two values: expectancy and standard deviation (E-SD). We use the Weibull noise index to estimate the noise in a voxel and to obtain more precise E-SD values for each voxel. We plot the frequency of voxels which have the same E-SD, then 3D segmentation based on the Weibull E-SD field is presented. Our test bed includes synthetic data as well as real volume data from a confocal laser scanning microscope (CLSM). Analysis of these data all show distinct and defining regions in their E-SD fields. Under the guide of the E-SD field, we can efficiently segment the objects embedded in real and simulated 3D data.

Index Terms—3D segmentation, Weibull E-SD field, noise index, confocal laser scanning microscope, CLSM.

1 Introduction

Many tasks in volume visualization involve exploring the inner structures of volume data. For example, a cell biologist may be interested in the structure of the microtubule spindle apparatus in an egg [1], [6]. The rapid increase in data set sizes required in order to collect images around the spindle apparatus, as well as the poor signal to noise ratio in the data set, make it difficult to extract geometric features efficiently. The work presented in this paper explores a coarse-grain approach to segmentation of volume data. Segmentation is a process of voxel classification that extracts regions by assigning the individual voxels to classes in such a way that these segmented regions posses the following properties: 1) voxels within the same region are homogeneous with respect to some characteristic (e.g., gray value or texture) and 2) voxels of neighboring regions are significantly different with respect to the same characteristic.

In this paper, the input data is on a 3D structured grid of vertices $v(i,j,k)$, each associated with a scalar value, and we consider a voxel as a cube including $\kappa \times \kappa \times \kappa$ 3D structured points, called a **κ-voxel**. Each κ-voxel is assigned two values: expectancy and standard deviation (E-SD). The expectancy in a voxel relates to its mean and the standard deviation indicates the variability of the data within it. We assume that the E-SD values of voxels in a region are relatively homogeneous and different from that in other regions. Many voxels have the same E-SD value. If we plot the frequency of voxels which have the same E-SD, then some areas in the E-SD domain will be dense and some sparse. We call this plot the **E-SD field** of the volume data. Obviously, for a given volume data, the E-SD field depends on the size of κ-voxels selected, i.e., the value of κ.

A simple and efficient way to calculate the E-SD is to compute its average and the sample standard deviation. However, noise makes it difficult to calculate the E-SD values accurately. Under this situation, the result of the E-SD plot is not stable and is dependent on a statistical model of the data [5]. A number of statistical frameworks have been proposed to model image and volumetric data. In [2], the observed image pixels were modeled as Rayleigh distribution random variables with means depending on their position. A Gaussian-function was used for pixel relaxation labeling in [3], [4], [11], [12], and [19]. Chesnaud et al. [5] instead proposed an exponential family of functions including Gaussian, Gamma, Rayleigh, and Possion to perform segmentation on 2D.

In this paper, a Weibull probabilistic framework for segmentation of Confocal Laser Scanning Microscope (CLSM) volume data is investigated. This distribution, first introduced in 1939 by W. Weibull, builds on empirical grounds in statistical theory of the strength of materials [15]. The Weibull distribution (WD) includes three parameters (see Section 2). An advantage of WD is that the WD kernel shape can be controlled by selecting different parameters for the gray levels of the input volume data.

In Section 2, we define spatially distributed objects, the Weibull distribution, the Weibull noise index, as well as discussing how to use it along with our algorithms. Section 3 shows 3D results from control data and two real CLSM volume data sets. Section 4 offers some concluding remarks.

- *J. Hu and A. Razdan are with the Partnership for Research in Stereo Modeling (PRISM), Arizona State University, Tempe, AZ 85287. E-mail: {hu.jiuxiang, razdan}@asu.edu.*
- *G.M. Nielson and G. Farin are with the Department of Computer Science, Arizona State University, Tempe, AZ 85287. E-mail: {nielson, farin}@asu.edu.*
- *D.P. Baluch and D.G. Capco are with the Department of Biology, Arizona State University, Tempe, AZ 85287. E-mail: {pag.baluch, dcapco}@asu.edu.*

Manuscript received 23 Aug. 2001; accepted 14 May 2002. For information on obtaining reprints of this article, please send e-mail to: tvcg@computer.org, and reference IEEECS Log Number 114841.

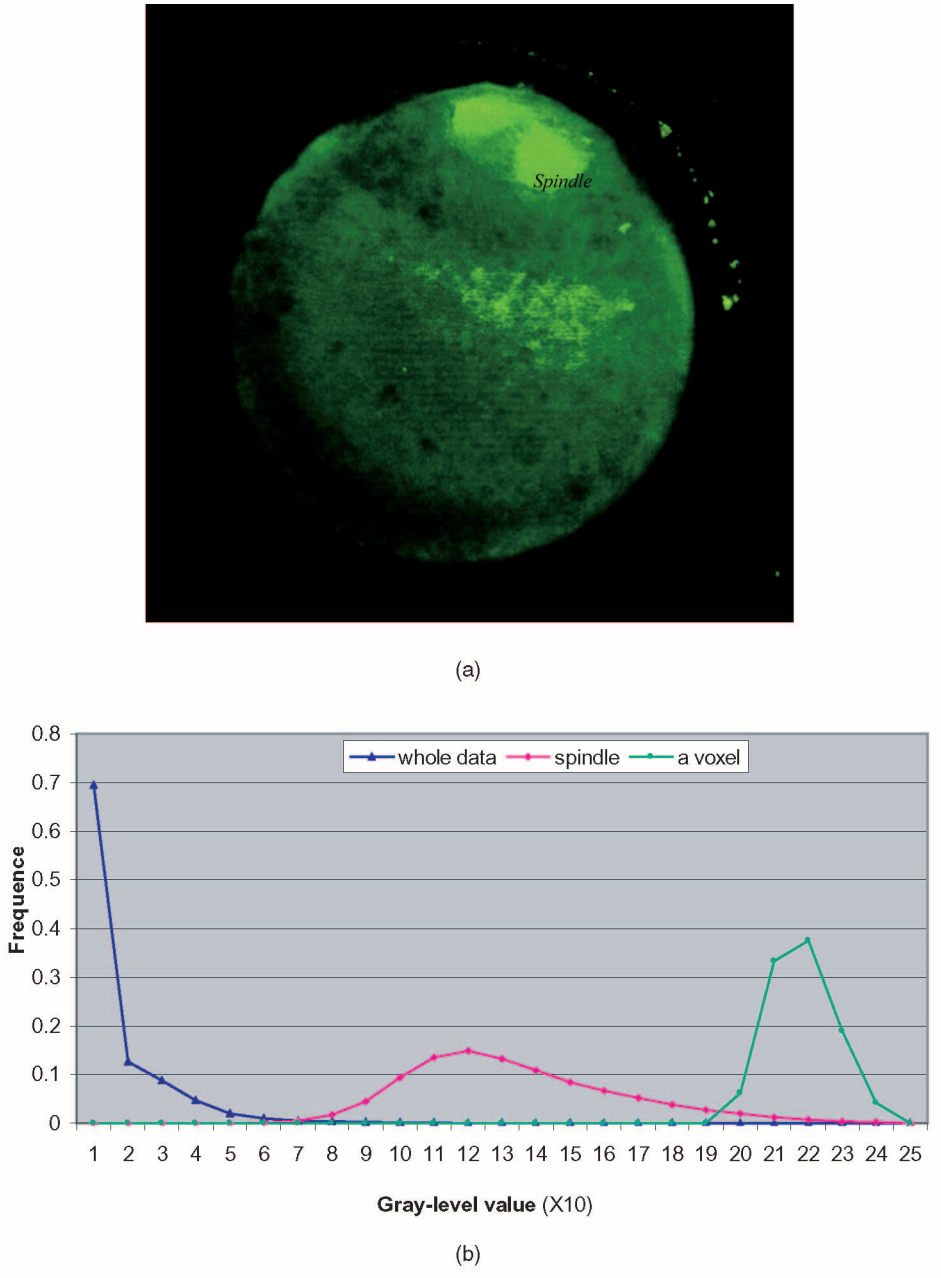

Fig. 1. Illustration of a distribution experiment using CLSM volume data. (a) A real CLSM volume data. (b) The distribution of the data in (a).

2 Models and Methods

2.1 Spatially Distributed Objects

Consider volumetric data $\mathbf{V}$, where the intensity of each image point $p = (i, j, k) \in \mathbf{V}$ is given by $v(i, j, k)$ or $v(p)$, whose size is $N = N_x \times N_y \times N_z$. In this paper, distribution means the probability of v over a certain interval $[a, b]$ $(b > a \geq 0)$. The random variable $X_\Omega(v)$ is the number of points in a region $\Omega \subseteq \mathbf{V}$ which have the value v, written as X_Ω. The density or frequency $f_\Omega(v)$ of a random variable X_Ω is defined as follows:

$$f_\Omega(v_0) = \frac{|\Omega_{v_0}|}{|\Omega|}, \tag{1}$$

where $\Omega_{v_0} = \{(i, j, k) \in \Omega | v(i, j, k) = v_0\}$, and $|\Omega|$ denotes the number of elements in Ω.

We assume that a homogeneous segment can be mathematically specified using two criteria: 1) the relative constant of regional expectancy and 2) the relative constant of regional variance of the intensity. These criteria are expressed as follows:

Definition 1. *A region Ω is called as a spatially distributed object (**SDO**), if the expectancy and standard deviation for each κ-voxel Δ in Ω are relatively constant, i.e.,*

$$E[X_\Delta] \in (e_1, e_2) \text{ and } SD[X_\Delta] \in (d_1, d_2), \tag{2}$$

where e_1, e_2, d_1, and d_2 denote predefined constants with $e_1 \leq e_2, d_1 \leq d_2$, the random variable X_Δ is defined as X_Ω above.

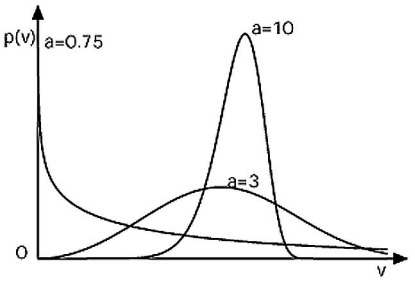

Fig. 2. Weibull distribution (5) with different shape parameters a and scale parameter $b = 1.2$ and $v_0 = 0$.

In general, the expressions of expectancy and standard deviation in a κ-voxel are given as follows [3], [13], [18]:

$$E[X_\Delta] = \frac{1}{|\Delta|} \sum_{(x,y,z)\in\Delta} v(x,y,z) = \sum_{v\in[a,b]} f_\Delta(v)v, \tag{3}$$

and

$$\begin{aligned} SD[X_\Delta] &= \sqrt{\frac{1}{|\Delta|} \sum_{(x,y,z)\in\Delta} v^2(x,y,z) - E^2[X_\Delta]} \\ &= \sqrt{\sum_{v\in[a,b]} f_\Delta(v)v^2 - E^2[X_\Delta]}, \end{aligned} \tag{4}$$

where f_Δ is defined by (1) in a κ-voxel and $|\Delta|$ denotes the number of elements in Δ. The SDOs are also called "agents" in [13] and called regions of interest (ROIs) in [12]. The goal of segmentation is to locate SDOs. The choice of e_1, e_2, d_1, and d_2 depends on the E-SD field.

However, if noise is present, then (3) and (4) will not give accurate E-SD values. We digress to describe the CLSM data which inherently includes noise and has a poor signal to noise ratio resulting in these inaccurate the E-SD values.

2.2 Confocal Laser Scanning Microscope Data Distribution

Confocal Laser Scanning Microscopy (CLSM) is a technique for obtaining high resolution scans of optical slices through a thick specimen without having to cut the specimen mechanically. Due to the precise lenses, the high coherency of the illuminating laser beam, and the confocal way of gathering backscattered light, accurate focusing at specific planar locations can be achieved. A typical optical section is between $0.1 \sim 100\mu m$. Scanning through the whole specimen thereby gives a full 3D projection view of the specimen. This technique is very useful not only because it allows the volumetric analysis of biological data, but also because the techniques used in "staining" these specimens (i.e., laser excited dyes) increase the accuracy of these images as compared to images obtained from ordinary optical microscopes. Nevertheless, images are still noisy and blurred. Several sources of noise can be identified [1], [7], [6]. These include:

1. thermal noise induced by the photomultiplier,
2. photon-shot-noise,
3. biological background (autofluorescence), and
4. unspecific staining.

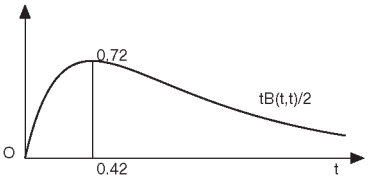

Fig. 3. The plot of function $tB(t,t)/2$. It reaches maximum 0.72 at $t = 0.42$.

The quality of the image can be affected by a possible mismatch of refractive indices, tissue scattering, dye concentration inside the cell, and the histological methods used for staining. These factors contribute to a position-dependent noise and blurring, which makes the analysis of these images rather difficult.

Statistical theory has been used for segmenting medical and biological data [2], [3], [19], [21], [22]. This assumes that the data follows a distribution. Hansen and Higgins assumed that intensity values in a region follow a Gaussian distribution in [4]. The Gaussian, Rayleigh, and Poisson distributions have been discussed separately in [5]. In our paper, before attempting to segment volume data using statistical theory, we first analyze the distribution. Fig. 1b shows the distribution of a CLSM data (see Fig. 1a). The plot marked with $\triangle$ shows the distribution of the complete volume data (see Fig. 1a), which looks like the Poisson distribution. The plot marked with $\diamond$ shows the distribution at the brightest region in Fig. 1a. This looks like a Gaussian distribution. The plot with $\circ$ illustrates the distribution in a 4-voxel. Based on the experiment, we will use Weibull distribution to model CLSM data because the Weibull model not only can approximate all distributions presented in CLSM data shown above by choosing its suitable parameter a, but also is a suitable model to remove noise in CLSM volume data.

2.3 Weibull Distribution

Weibull distribution is defined as follows [15]:

$$p(v) = \frac{a}{b}\left(\frac{v-v_0}{b}\right)^{a-1} \exp\left[-\left(\frac{v-v_0}{b}\right)^a\right], \tag{5}$$

where $v \geq v_0$, $a > 0$ is the shape parameter, $b > 0$ is the scale parameter, and v_0 is the shift parameter (the minimum possible value of the random variable). In the CLSM data, the minimum possible density value is zero, i.e., $v_0 = 0$. Therefore, we assume that the shift parameter of the Weibull distribution is 0 in the rest of this paper. Fig. 2 gives the Weibull distribution (5) with different shape parameters a and scale parameter $b = 1.2$ and $v_0 = 0$. The expectancy and the deviation of the random variable X obeying the Weilbull distribution are given by:

$$E[X] = b\Gamma\left(1+\frac{1}{a}\right), \tag{6}$$

and

$$SD^2[X] = b^2\left[\Gamma\left(1+\frac{2}{a}\right) - \Gamma^2\left(1+\frac{1}{a}\right)\right], \tag{7}$$

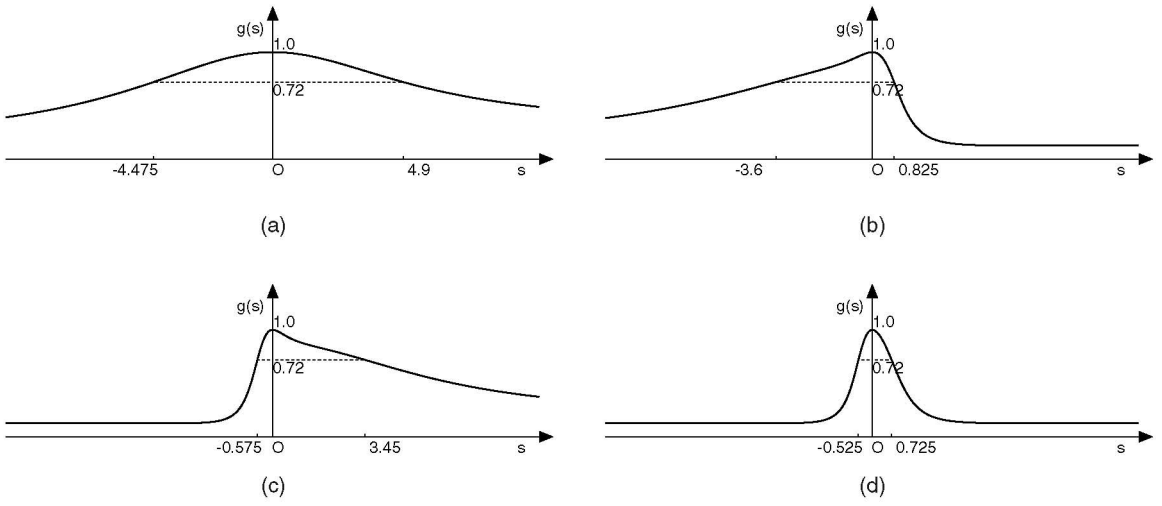

Fig. 4. Illustration of the classification of noise in a 2-voxel by using two parameters: s_1 and s_2 are defined by Definition 2. (a) Normal sample case: $\{64, 52, 64, 46, 50, 54, 62, 43\}$, where $s1 = 4.475$ and $s2 = 4.9$. (b) Upper noise case $\{240, 52, 64, 46, 50, 54, 62, 43\}$, resulted from case (a) when one upper noise term was added, where $s_1 = 0.825$ and $s_2 = 3.6$. (c) Lower noise case $\{6, 52, 64, 46, 50, 54, 62, 234\}$, resulted from case (a) when one lower noise term was added, where $s_1 = 3.45$ and $s_2 = 0.575$. (d) Lower noise case $\{6, 52, 64, 46, 50, 54, 62, 234\}$, resulted from case (a) when one low noise term and one upper noise term were added, where $s_1 = 0.725$ and $s_2 = 0.525$.

where the gamma function is $\Gamma(x) = \int_0^\infty t^{x-1}e^{-t}dt$. It can be shown that, when $a = 1.0$, it is the Possion pdf and, when $a = 2.0$, one has the Rayleigh pdf and, when $a = 3.0$, it turns into the Gaussian pdf. When $a \gg 1$, the distribution tends to be a uniform pdf. Therefore, the Weibull model is a suitable model to fit the histogram distribution of these volume data and the regions within them whose statistical properties are unknown since the kernel shape can be controlled by selecting a different a value.

From (6) and (7), it is clear that the parameters a and b of the WD depend on the expectancy and the standard deviation. We denote the ratio $r = SD/E$ in (6) and (7) with $v_0 = 0$ and the relationship between r and the shape parameter a of its Weibull distribution is as follows:

$$r^2 = \frac{SD^2[X]}{E^2[X]} = \frac{\Gamma(1 + 2/a)}{\Gamma^2(1 + 1/a)} - 1, \tag{8}$$

or

$$\frac{1}{r^2 + 1} = \frac{\Gamma^2(1/a)}{2a\Gamma(2/a)} = \frac{1}{2a}B(1/a, 1/a) \doteq \frac{1}{2}tB(t, t), \tag{9}$$

where the Beta function is $B(x, y) = \int_0^1 t^{x-1}(1 - t)^{y-1}dt$, a is the shape parameter of the WD, and $t = 1/a$. From (9), we can see that the shape parameter of the Weibull distribution is only dependent on ratio r in the E-SD field. When $t \approx 0.42$, the RHS of (9) reaches its maximum, which is near the value 0.72. Unfortunately, the RHS of (9) is not a monotonic function of t (see Fig. 3). In order to overcome this difficulty, we first give some properties of the Weibull distribution [15].

Property 1. *For every $s > 0$, the s-moment of Weibull distribution is*

$$E[X^s] = b^s\Gamma(1 + s/a). \tag{10}$$

Property 2. *If $X_1, X_2, \cdots, X_n$ are independent distribution random variables and follow the Weibull law, then*

$$\frac{1}{n}\sum_{i=n}^{n} X_i^s \to E[X^s], \ for\ 1 \le s < \infty, \ as\ n \to \infty. \tag{11}$$

2.4 Weibull Noise Index

Removing noise or improving the signal-to-noise ratio (SNR) of a given image is an essential step in segmentation, especially in high noise situations that can disrupt the shape and lose the edge information. The traditional algorithms of denoising, such as Gaussian filter [8], [20], reduce the noise, but they do not maintain the edge information. When noise is removed, it is required to not only smooth all of the homogenous regions that contain noise, but also to keep the position of boundaries, i.e., not to lose the edge information that defines the structure of objects.

Let $v_1, v_2, \cdots, v_{\kappa^3}$ represent κ^3 image points in a given κ-voxel. It is assumed that the value of a voxel is characterized by the Weibull distribution. If we use (3) and (4) to calculate the E-SD value, the results are not reliable due to noise, especially for a standard deviation [18], [20]. Therefore, we must find a way to distinguish whether or not the data distribution in a κ-voxel is uniform. If it is not uniform, then what kind of noise is present? If few of the elements in a voxel are significantly larger and/or smaller than others, then these are called **upper/lower noise**. For example, in a 2-voxel, in which the set of the intensity at eight image points is $\{234, 52, 64, 46, 50, 54, 62, 3\}$, element 234 is much larger than others, and is called an upper noise. Element 3 is significantly less than others and is called a lower noise. In order to classify the noise in a κ-voxel, an auxiliary function $g(s)$ is introduced:

$$g(s) = \frac{\left(\sum_{i=1}^{n} v_i^s\right)^2}{n\sum_{i=1}^{n} v_i^{2s}}, \tag{12}$$

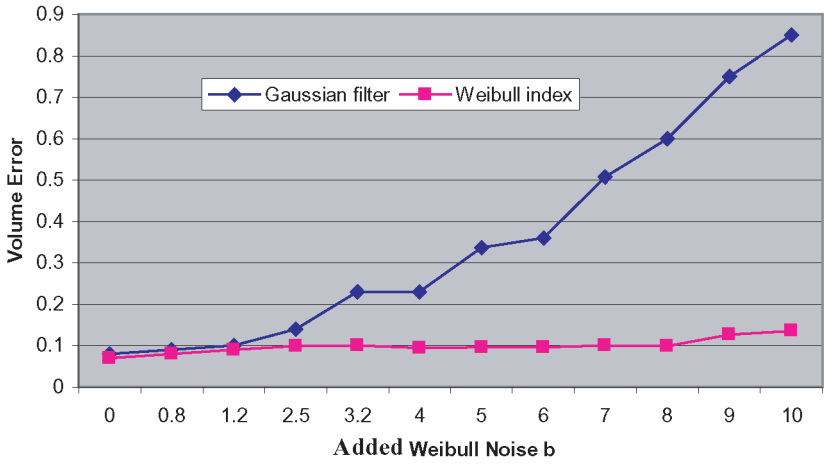

Fig. 5. Volume error comparison between Gaussian filter and Weibull noise indices in segmenting the synthetic volume data.

where $s \in (-\infty, \infty)$, $v_i > 0$ $(1 \le i \le n)$, and $n = \kappa^3$. By calculating (12) directly, we have the derivative of the function $g(s)$ that satisfies: $g'(s) \le 0$ for $s > 0$, $g'(s) \ge 0$ for $s < 0$, and $g'(s) \le 0$ if and only if $v_1 = V_2 = \cdots = v_n$. Also: $g(0) = 1$, $g(\infty) = \frac{k_1}{n}$, and $g(-\infty) = \frac{k_2}{n}$, where k_1 is the number of the elements which are equal to the maximum and k_2 is the number of the elements which are equal to the minimum. It is obvious that $1 \le k_1, k_2 \le n$ and $k_1 + k_2 \le n$.

Using Properties 1 and 2, we know that

$$g(s) \approx \frac{(E[X^s])^2}{E[X^{2s}]} = \frac{1}{2} t_s B(t_s, t_s),$$

where $t_s = s/a$ and a is the WD shape parameter in the κ-voxel. From the analysis above, the function $t_s B(t_s, t_s)/2$ reaches its unique positive maximum near 0.72 at $t_s = 0.42$. If k_1 and k_2 are small enough ($k_1, k_2 \le \lfloor 0.14n \rfloor$ [1]) and there is an s_0 such that $g(s_0) = 0.72$, then we have that the WD shape parameter in a κ-voxell satisfies

$$a \approx s_0/0.42. \tag{13}$$

Definition 2. *If $s_1 > 0$ such that $g(s_1) = 0.72$ (if $k_1 > 0.72n$, set $s_1 = \infty$), then s_1 is called the Weibull upper noise index. If $s_2 > 0$ such that $g(-s_2) = 0.72$ (if $k_2 > 0.72n$, set $s_2 = \infty$), then s_2 is called the Weibull lower noise index. In short, they are called the Weibull noise indices.*

We will use these two parameters to determine the "goodness" of voxel distribution as follows (see Fig. 4):

- For a κ-voxel, if the Weibull upper noise index $s_1 < 1.26$ and the lower noise index $s_2 > 1.26$, then there is upper noise in it.
- For a κ-voxel, if the Weibull upper noise index $s_1 > 1.26$ and the lower noise index $s_2 < 1.26$, then there is lower noise in it.
- For a κ-voxel, if the Weibull upper noise index $s_1 < 1.26$ and the lower noise index $s_2 < 1.26$, then there is upper and lower noise in it.

1. $\lfloor x \rfloor$ is the maximum integer which is less than x.

2.5 Segmentation Algorithm

Based on the theoretical analysis above, the algorithm for volume data segmentation is as follows:

Step 1: Given a κ to determine the size of κ-voxel; initialize the SDO's predefined constant in (2): $e_2 > e_1 > 0$, $d_2 > d_1 \ge 0$, and the threshold of expectancy $T_e > 0$.

Step 2: Consider the jth κ-voxel. Use bisection to compute its Weibull noise index s_1 and s_2, which are the roots of the equation $g(s) = 0.72$, where $g(s)$ is defined by (12). If there is upper noise or lower noise or both, then remove the noise directly (i.e., delete the minimum or the maximum or both). Repeat at most $\lfloor C\kappa^3 \rfloor$ times to execute Step 2.

Step 3: Calculate E-SD values using (3) and (4). If the expectancy is larger than the threshold T_e, add the κ-voxel to list $\mathcal{A}$. If there are κ-voxels which have not been dealt with, then go to Step 2.

Step 4: Compute the frequency of the voxel in the list $\mathcal{A}$ and create the E-SD field. By choosing the suit E-SD values $e_2 > e_1 > 0$, $d_2 > d_1 \ge 0$, select the voxel in which the expectancy E and standard deviation SD satisfy: $e_2 \ge E \ge e1$, $d_2 \ge SD \ge d_1$.

In this algorithm, the threshold T_e is used for controlling the size of list $\mathcal{A}$ above and will cause the image to be rendered faster. The constant C in **Step 2** is equal to 0.14. E-SD values $(e_2, e_1; d_2, d_1)$ define a movable rectangle, called a **window** in the E-SD field. The suit E-SDs ($e_2 > e_1$, $d_2 > d_1$) are determined through user interaction by moving its left-top and/or right-bottom vertices (see Fig. 6i).

The algorithm described above is simple and efficient. Its average complexity is $O(L \log L)$ for each selection by moving window, where L is the number of κ-voxels, defined by $L = N/\kappa^3$, where N is the number of points in the volume data. Obviously, if the grains (or κ-voxels) are coarser (i.e., κ is larger), then the selection is more efficient; however, the results of the segmentation will also be coarser. With different κ ($\kappa = \kappa_{\min}, \cdots, \kappa_{\max}$, $\kappa_{\min}$ and $\kappa_{\max}$ are prespecified), the selected κ best fits the given volume data. By this fitting approach, the number of SDOs in

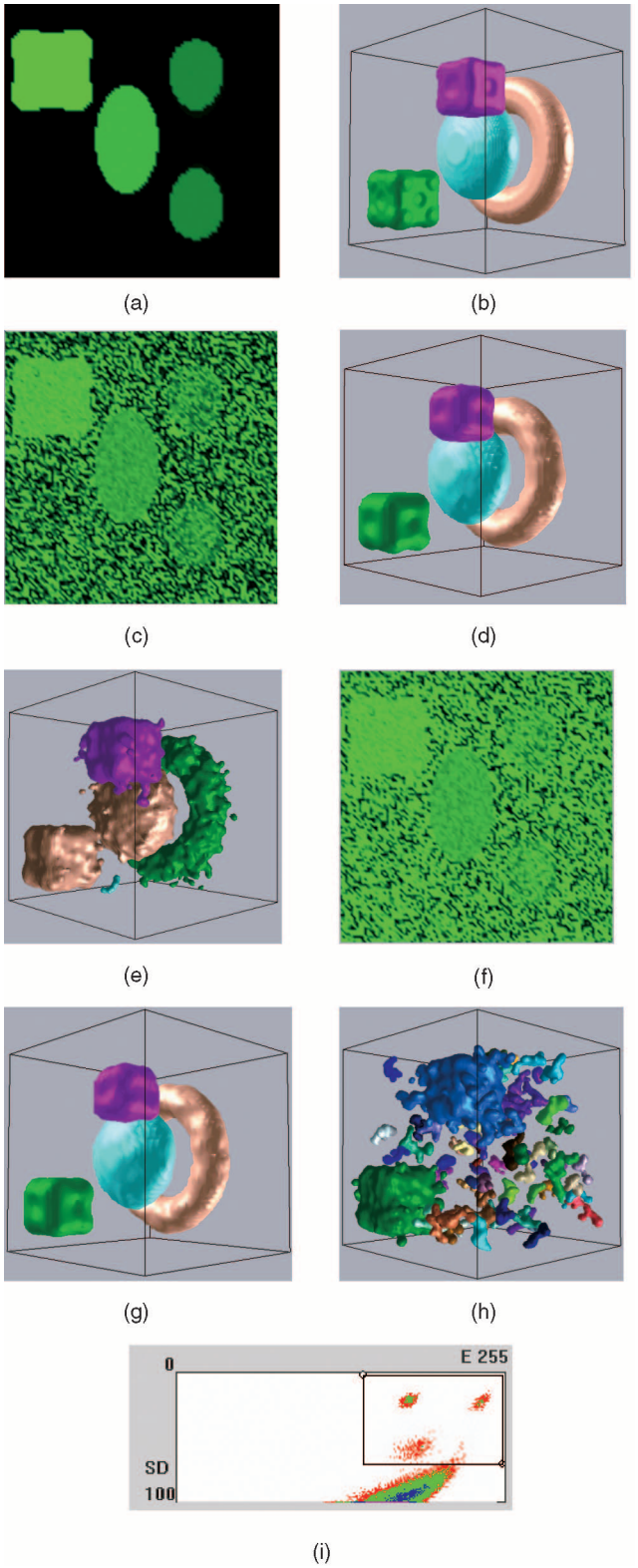

Fig. 6. Segmentation results for different noise-added control volume data. (a) A slice of noise-free data as a reference. (b) The segmentation of reference data. (c) A slice of noise-added data with $b = 5.0$. (d) Segmentation using our method. (e) Segmentation using Gaussian filter $\sigma = 1.3$. (f) A slice of noise-added data with $b = 10.0$. (g) Segmentation using our method. (h) Segmentation using Gaussian filter $\sigma = 1.3$. (i) Weibull E-SD field of the noise-added volume data with Weibull scale parameter $b = 10.0$.

volume data is determined. The minimum κ, which shows the number of SDOs in E-SD field, will be chosen.

3 Examples

In this section, we will look at two examples illustrating the proposed method for segmentation. The first example examines artificial volume data generated using a Weibull distributed random number with different parameters. The second example uses real CLSM data from two different data sets and demonstrates how this model can be used to segment such data. The hardware we used is a Dell Precision workstation 330, with P4 1.4GHz CPU and 1-GB RAM.

3.1 Controlled Experiment

In order to make the experiment comparable, a controlled experiment is done in the following way: We first segment a noise-free volume data (see Fig. 6a) and treat that segmentation as our reference, which includes a torus, an ellipsoid, and two deformed cubes of different sizes, but with the same shape parameter a, in a $100 \times 100 \times 100$ cube (see Fig. 6b). Every instance of a volume data with added noise is then denoised using a Gaussian filter with $\sigma = 1.3$ and a Weibull noise index with 2-voxels or 3-voxels. The targets are then segmented from these images and compared to the reference objects. The comparison, based on the segmented volume, is done by identifying the support function of the reference object and of the object segmented from a volume data with added noise, denoted by S_r and S_n, respectively. That is, $S_\xi = 1$ or 0 if x is in the segmented objects or not, where $\xi = \{r, n\}$. Then, the volume deviation (error) of S_n from S_r in the volume data $\mathbf{V}$ is defined as follows:

$$\delta(S_n, S_r) = \frac{\sum_{x \in \mathbf{V}} |S_r(x) - S_n(x)|}{\sum_{x \in \mathbf{V}} S_r(x)}. \tag{14}$$

These deviations are calculated to produce numbers that are comparable across different noise levels. Several levels of noise have been added to the test volume data to show the robustness of the filter. The noise that is added to every image point is a Weibull distributed random number: $Y = \min\{255, C[-b \ln(1 - X)^{1/a}]\}$, with different scale parameters b, where random variable X is the uniform distribution in $[0, 1]$, a is the Weibull shape parameter, and C is a constant for each object. Finally, the volume error from the simulated volume data is plotted in Fig. 5. As depicted in Fig. 5, the volume error corresponding to the Weibull noise index is significantly lower compared to those that result from applying a Gaussian filter and the Weibull noise index is robust to noise. Segmentation results are shown in Fig. 6.

Fig. 6i shows the Weibull E-SD field of the noise-added volume data with the scale parameter $b = 10.0$. The colors in the E-SD field correspond to frequency. We denote by $N(e, d)$ the number of the κ-voxels whose expectancy is e and standard deviation is d. The color at point (e, d) in the E-SD field is determined by $\log(N(e, d))$. We set the color at point (e, d) as follows:

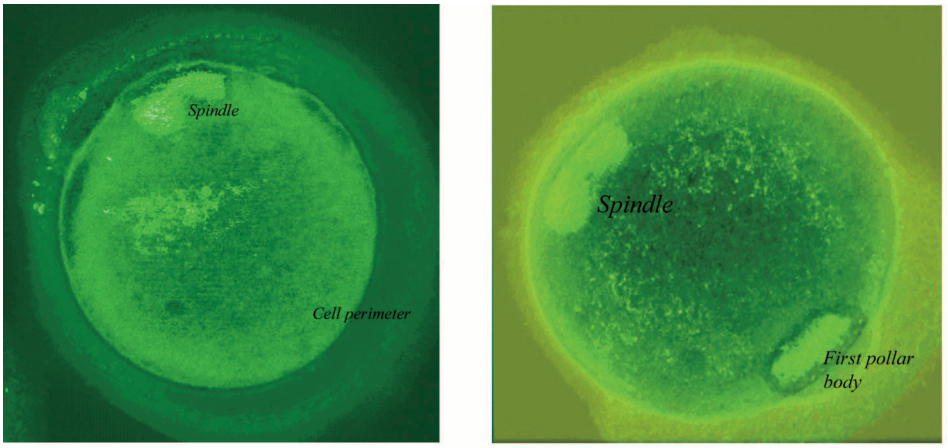

Fig. 7. Test bed for our Weibull E-SD modeling scheme. The images come from two different data sets. In both images, there is only one cell and its spindle is at the up part of the cell (labeled by a biologist). The size of image (a) is $512 \times 512 \times 124$; its gray-level is from 0 to 255. The size of image (b) is $512 \times 512 \times 146$; it has the same gray-level as (a).

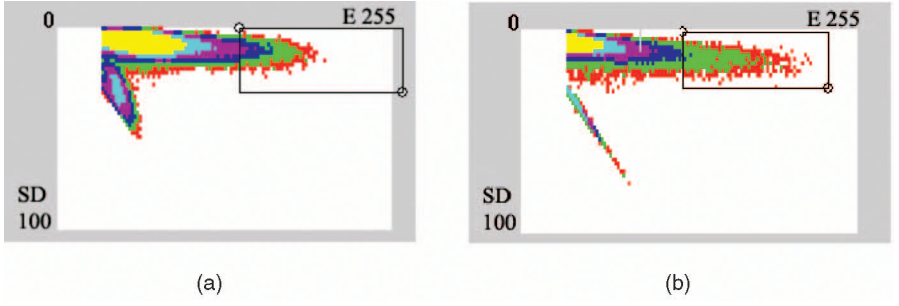

Fig. 8. The Weibull E-SD fields from the data shown in Fig. 7. The colors have the same mean as in Fig. 6i. In(a), the size of the window is $(178, 237; 4, 27)$, corresponding to the segmentation shown in Fig. 9a. The threshold T_e is 34, which creates a blank on the left side. There are two clear regions. In (b), the size of the window is $(167, 255; 2, 30)$, corresponding to the segmentation shown in Fig. 9b. The threshold T_e is 34, which creates a blank on the left side. There are two clear regions, too. (a) The Weibull E-SD field of the image in Fig. 7a. (b) The Weibull E-SD field of image in Fig. 7b.

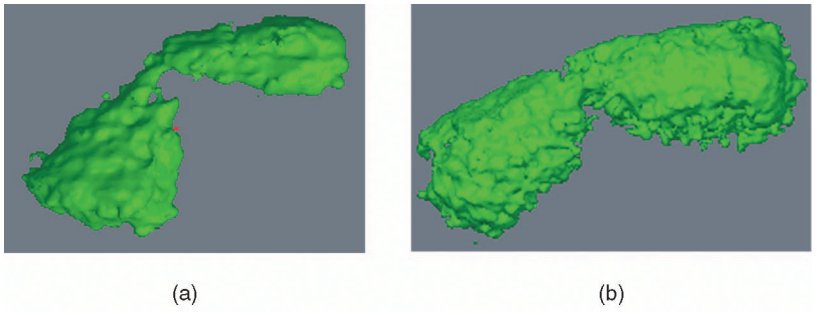

Fig. 9. The spindle segmentation corresponding to Fig. 7. The segmentation in (a) includes 3,902 boxes and 11,308 boxes in (b).

$$c = \begin{cases} RGB(255,255,255), & \text{if } 0.0 \le \log(N(e,d)) < 0.5 \\ RGB(255,0,0), & \text{if } 0.5 \le \log(N(e,d)) < 1.0 \\ RGB(0,255,0), & \text{if } 1.0 \le \log(N(e,d)) < 1.5 \\ RGB(0,0,255), & \text{if } 1.5 \le \log(N(e,d)) < 2.0 \\ RGB(255,0,255), & \text{if } 2.0 \le \log(N(e,d)) < 2.5 \\ RGB(0,255,255), & \text{if } 2.5 \le \log(N(e,d)) < 3.0 \\ RGB(255,255,0), & \text{if } 3.0 \le \log(N(e,d)). \end{cases} \quad (15)$$

The colors in the E-SD field of real CLSM data below have the same meanings. Next, the left-top and right-bottom vertices of window in the E-SD field, which give the values $(e_2, e_1; d_2, d_1)$, define the range of expectancy and standard deviation of a SDO (see Fig. 6i).

Fig. 6c shows a slice of the noise volume data with the Weibull scale parameter $b = 5.0$. The segmentation results, using our method and threshold method with Gaussian filter, are given in Fig. 6d and Fig. 6e. Although it has lost some detail information, such as the deformation in the two cubes compared with the reference Fig. 6b, the segmentation using our method keeps the number[2] and shape of objects. In contrast, segmentation performed by using threshold methods with Gaussian filter lost the number

2. Different components are colored using different colors.

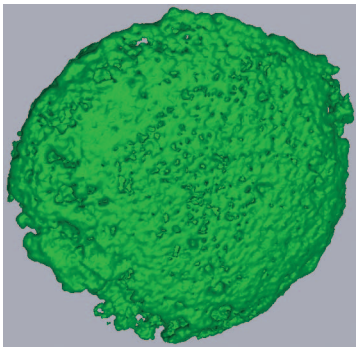

Fig. 10. The segmented area corresponding to the smaller region in Fig. 8a.

and shape of the objects. Fig. 6f shows a slice of the noise volume data with the Weibull scale parameter $b = 10.0$ and the segmentation results from this noise data using our method and the threshold method with a Gaussian filter are given in Fig. 6g and Fig. 6h. Fig. 6i shows the Weibull E-SD field of this noise volume data, and illustrates that the three different components present. Using our segmentation method maintains the number and shape of the objects, but using threshold techniques with Gaussian filter fails in segmenting the objects.

3.2 CLSM Data

In this example, we use data from two different CLSM data sets designed for investigating the meiotic spindle within a mouse egg. The eggs were viewed on the Leica TCS NT confocal microscope. Multiple lasers allow for simultaneous imaging of the DAPI (Argon UV [363 nm]) and ALEXA 568 Krypton[568 nm]) fluorophore-labeled samples. Using a 63x water objective, images were scanned between $0.2 \sim 0.4\mu m$ intervals along the z-axis, 0.154 μm along the xy-axis and collected through the volume of the entire egg.

Fig. 7 shows a CLSM test bed for our Weibull E-SD modeling scheme from different experiments. The data in Fig. 7a is collected using a Krypton laser and highlights regions targeted with an antibody to anti-a-tubulin at the upper left and brighter regions through the egg. The image in Fig. 7a shows a meiotic metaphase II arrested egg and is composed of 124 slices within a 512×512 matrix, contains a gray-level from 0 to 255. The size of the data shown in Fig. 7b is $512 \times 512 \times 146$ and has the same gray-level range as in Fig. 7a. In Fig. 7b, the egg has a meiotic spindle at the upper left and the remains of the primary polar body at the bottom right. Fig. 8 shows the E-SD plots of Fig. 9. The colors have the same meanings as in Fig. 6i. In Fig. 8a, the size of the window is $(170, 237; 4, 27)$, corresponding to the segmentation of the data shown in Fig. 9a. In Fig. 8b, the size of the window is $(183, 255; 2, 30)$ corresponding to the segmentation of the data shown in Fig. 9b. We set the threshold at $T_e = 34$, and $\kappa = 2$. The segmentation in Fig. 9a includes 3,902 voxels, and 11,308 voxels in Fig. 9b.

What gives rise to such clear *regions* in the Weibull E-SD field shown in Fig. 8 is unknown. A plausible explanation is that each region corresponds to a SDO. When we move the window on Fig. 8a to the small region, an area of cell perimeter in Fig. 7a is segmented (see Fig. 10).

4 Conclusions

We have proposed a coarse-grain approach for the segmentation of an object from volume data based on the Weibull E-SD field. We have shown that one can decide the noise index in a κ-voxel by using the Weibull law and use the E-SD field as a guide to segment an object. We have consistently demonstrated this approach on controlled as well as on real volume data.

One of the remaining limitations of the present approach is that it is still semi-automatic and consequently requires the intervention and expertise of a user. It would be desirable to move in the direction of a more fully automatic segmentation procedure.

Acknowledgments

This work was supported by the US Defense Advanced Research Projects Agency (MDA 972-00-1-0027) and the US National Science Foundation (IIS-998016 and ACI-0083609) and the US National Institutes of Health (HD 32621) and the US Office of Naval Research (N00014-00-1-0281 and N00014-02-1-0287). The authors would like to thank PRISM, the W.M. Keck BioImaging Laboratory, and the Cell Biology Laboratory at Arizona State University for providing the data and computing resources.

References

[1] A. Razdan, K. Patel, G. Farin, and D.G. Capco, "Visualization of Multicolor CLSM Data Set," *Computers and Graphics*, vol. 25, no. 3, pp. 371-382, 2001.

[2] J.M.B. Dias and J.M.N. Leitao, "Wall Position and Thickness Estimation from Sequences of Echocardiographic Images," *IEEE Trans. Medical Imaging*, vol. 15, no. 1, pp. 25-38, Jan. 1996.

[3] R.A. Hummel and S.W. Zucker, "On the Foundations of Relaxation Labeling Processes," *IEEE Trans. Pattern Analysis and Machine Intelligence*, vol. 5, no. 3, pp. 267-287, Mar. 1983.

[4] M.W. Hansen and W.E. Higgins, "Relaxation Methods for Supervised Image Segmentation," *IEEE Trans. Pattern Analysis and Machine Intelligence*, vol. 19, no. 9, pp. 949-962, Sept. 1997.

[5] C. Chesnaud, P. Refregier, and V. Boulet, "Statistical Region Snake-Based Segmentation Adaped to Different Physical Noise Models," *IEEE Trans. Pattern Analysis and Machine Intelligence*, vol. 21, no. 11, pp. 1145-1157, Nov. 1999.

[6] M.H. Fox, D.J. Arndt-Jovin, T.M. Jovin, and P.H. Baumann, "Robert-Nicoud, M. Spatial and Temporal Distribution of DNA Replication Sites Localized by Immunoflurescence and Confocal Microscopy in Mouse Fibroblast," *J. Cell Science*, vol. 99, pp. 247-253, 1991.

[7] E.M.M. Manders, J. Stap, G.J. Brakenhoff, R. van Driel, and J.A. Aten, "Dynamics of Three Dimensional Replication Patterns During the S-Phase, Analyzed by Double Labeling of DNA and Confocal Microscopy," *J. Cell Science*, vol. 103, no. 3, pp. 857-862, 1992.

[8] W.E. Higgins and E.J. Ojard, "Interactive Morphological Watershed Analysis for 3D Medical Images," *Computer Medical Imaging Graphics*, special issue on advanced 3D image processing in medicine, vol. 17, nos. 4/5, pp. 387-392, 1993.

[9] C. Garbay, "Image Structure Representation and Processing: A Discussion of Some Segmentation Algorithms in Cytology," *IEEE Trans. Pattern Analysis and Machine Intelligence*, vol. 8 no. 2, pp. 140-146, Feb. 1986.

[10] P.W. Fung, K.K. Ly, and K. Attikiouzel, "Automatic Segmentation of Biomedical Images," *Proc. IEEE Conf. Acoustics, Speech, and Signal Processing*, pp. 882-885, 1988.

[11] A. Rosenfeld, R. Hummel, and S.W. Zucker, "Science Labeling by Relaxation Operations," *IEEE Trans. Systems, Man, and Cybernetics*, vol. 6, no. 6, pp. 420-433, 1976.

[12] M. Svensen, F. Kruggel, and D.Y. Cramon, "Probabilistic Modeling of Single-Trial fMRI Data," *IEEE Trans. Medical Imaging,* vol. 19, no. 1, pp. 25-35, Jan. 2000.
[13] J. Liu and Y. Tang, "Adaptive Image Segmentation with Distributed Behavior-Based Agents," *IEEE Trans. Pattern Analysis and Machine Intelligence,* vol. 21, no. 6, pp. 544-551, June 1999.
[14] L. Andrews, *Special Functions of Mathematics for Engineers,* second ed. McGraw-Hill, 1992.
[15] E. Suhir, *Applied Probability for Engineering and Science.* McGraw-Hill, 1997.
[16] N. Sarkar and B.B. Chaudhuri, "An Efficient Differential Box-Counting Approach to Computer the Fractal Dimension of Images," *IEEE Trans. Systems, Man, and Cybernetics,* vol. 24, no. 1, pp. 115-120, Jan. 1994.
[17] M. Kamber, R. Shinghal, and D.L. Collins, "Model-Based 3-D Segmentation of Multiple Sclerosis Lesions in Magnetic Resonance Brain Images," *IEEE Trans. Medical Imaging,* vol. 14, no. 3, pp. 442-453, Mar. 1995.
[18] B. Chanda, B.B. Chaudhuri, and D.D. Majumde, "A Modified Scheme for Segmenting Noisy Images," *IEEE Trans. Systems, Man, and Cybernetics,* vol. 18, no. 3, pp. 458-466, Mar. 1988.
[19] A. Chakraborty and J.S. Duncan, "Game-Theoretic Integration for Image Segmentation," *IEEE Trans. Pattern Analysis and Machine Intelligence,* vol. 21, no. 1, pp. 12-30, Jan. 1999.
[20] T.C.M. Lee, "Segmentation Images Corrupted by Correlated Noise," *IEEE Trans. Pattern Analysis and Machine Intelligence,* vol. 20, no. 5, pp. 481-492, May 1998.
[21] A.D. Lanterman, U. Grenander, and M.I. Miller, "Bayesian Segmentation via Asymptotic Partition Functions," *IEEE Trans. Pattern Analysis and Machine Intelligence,* vol. 22, no. 4, pp. 337-347, Apr. 2000.
[22] J. Berkmann and T. Caelli, "Computation of Surface Geometry and Segmentation Using Covariance Techniques," *IEEE Trans. Pattern Analysis and Machine Intelligence,* vol. 16, no. 11, pp. 1114-1116, Nov. 1994.
[23] G.M. Nielson, M. Gross, H. Hagen, and S.V. Klimenko, "Research Issues in Data Modeling for Scientific Visualization," *IEEE Computer Graphics and Applications,* vol. 14, no. 2, pp. 70-73, 1994.

Jiuxiang Hu received the BS, MS, and PhD degrees in mathematics from Huazhong Normal University in 1988, Huazhong University of Science and Technology in 1991, and Lanzhou University, China, in 1994, respectively. He has been an assistant research scientist in the PRISM Lab at Arizona State University since 2000. Since receiving the PhD degree, he was a postdoctoral fellow from 1995 to 1996 and then joined the Department of Computer Science, Huazhong University of Science and Technique, where he was promoted to an associate professor in 1997. His research interests include computer graphics, visualization, image processing, and expert systems. He has developed and implemented methods to segment biomedical volume data sets, including image statistical modeling and segmentation techniques with application to structural and quantitative analysis of 3D images.

Anshuman Razdan received the BS and MS degrees in mechanical engineering and PhD degree in computer science.He is the director of PRISM: Partnership for Research In Stereo Modeling at Arizona State University. His research interests include computer-aided geometric design (CAGD) and computer graphics, NURB curves and surfaces approximation, feature segmentation for surface and volume data, and use of high bandwidth networking for scientific visualization. He is a PI on several US National Science Foundation grants, including a recent $2.1 M KDI grant on 3D Knowledge: Acquisition, Representation, and Analysis (3DK). He is a member of the IEEE.

Gregory M. Nielson is a professor of computer science and affiliate professor of mathematics at Arizona State University. He has lectured and published widely in the areas of computer-aided geometric design and scientific visualization. He has collaborated with several institutions, including NASA, Xerox, General Motors, and LLNL. Professor Nielson is or has been on the editorial boards of several professional journals, including the *Rocky Mountain Journal of Mathematics*, *Computer Aided Geometric Design*, *Visualization and Computer Animation Journal*, *Computer Graphics*, *IEEE Computer Graphics and Applications*, and *ACM Transactions on Graphics*. He is one of the founders and members of the steering committee of the IEEE sponsored conference series on Visualization. He has previously chaired and is currently a director of the IEEE Computer Society Technical Committee on Computer Graphics. He cofounded the *IEEE Transactions on Visualization and Computer Graphics*. He has received an IEEE Meritorious Service Award, an IEEE Outstanding Contribution Award, and the John Gregory Memorial Award in Geometric Modeling for his pioneering research efforts in CAGD. He is a senior member of the IEEE.

Gerald Farin received the PhD degree from the University of Braunschweig, Germany, in 1979. He is a professor of computer science at Arizona State University. His interests are curve and surface modeling. He has written several books and other publications on this topic.

D. Page Baluch received the BA degree in biology from the University of Colorado at Colorado Springs in 1999. She is currently pursuing the PhD degree in biology at Arizona State University. She works as a research assistant in the Partnership for Research in Stereo Modeling (PRISM) lab and conducts her graduate studies in the Molecular and Cellular Biology lab of Dr. David Capco in the Biology Department. Her current interests are studying the cytoskeletal elements involved in the signal transduction pathways of mouse eggs before and after fertilization.

David G. Capco received the PhD from the University of Texas at Austin in cell and developmental biology (1980) and underwent further training during his postdoctoral work at MIT before becoming a member of the faculty at Arizona State University in 1984. He is a professor of biology at Arizona State University. His research interests focus on the signal transduction machinery that regulate cell function with an emphasis on signaling agents which regulate the cell cycle, specifically in mammalian eggs. His research examines mechanisms to increase the efficiency of cloning of agricultural animals.